CSMA 2026
17ème Colloque National en Calcul des Structures
18-22 Mai 2026, Presqu'île de Giens (Var)

Polytopal discretisation of a quasi-dynamic poromechanical induced seismicity model

M. E.A. Zerga[1], R. Masson[2], J.-P. Ampuero[3]

[1] *Mohammed El-Hadi Zerga, Université Côte d'Azur, CNRS, LJAD, Nice, France, mohammed-el-Hadi.zerga@univ-cotedazur.fr*
[2] *Roland Masson, Université Côte d'Azur, Inria, CNRS, LJAD, team Galets, Nice, France, roland.masson@univ-cotedazur.fr*
[3] *Jean-Paul Ampuero, Université Côte d'Azur, CNRS, IRD, OCA, Geoazur, Sophia-Antipolis, France, ampuero@geoazur.unice.fr*

Résumé —
This work addresses the polytopal discretisation of an induced seismicity model accounting for fault reactivation and slip driven by subsurface fluid injection. The model couples single-phase Darcy flow in both the porous matrix and the fault network with a poroelastic mechanical response in the bulk and fault slip governed by a rate-and-state friction law. The contact mechanics problem is discretised using the Virtual Element Method with bubble stabilisation of the Lagrange multiplier. It is combined with a Hybrid Finite Volume scheme for the mixed-dimensional Darcy flow model.
Mots clés — Rupture dynamics, induced seismicity, polytopal discretisation, Virtual Element Method, adaptive time stepping

1 Introduction

Subsurface resources such as deep geothermal energy, underground hydrogen storage, and geological CO2 sequestration have become crucial pillars of the energy transition and sustainable development. However, injecting or extracting fluids into or from the subsurface modify the pressure and stress state of the surrounding rocks, often extending far beyond the injection point. These changes can potentially trigger fault reactivation, including earthquakes (see Figure 1). Such phenomena pose seismic risks that must be better understood and mitigated to ensure operational safety, reduce risks to nearby populations, and enhance the social acceptance of these projects. If it remains sufficiently low, this induced seismicity (then referred to as microseismicity) raises no issue and can even contribute to site monitoring. However, the ability to predict and mitigate the risks of induced seismicity is key for sustainable exploitation of the subsurface. In recent years, anthropogenic activities in storage reservoirs have triggered earthquakes with magnitudes up to 6, high enough to cause damage, in regions where natural seismic activity was otherwise low. A recent example is a magnitude 3.9 earthquake in Vendenheim, Alsace, which led to the closure of this deep geothermal site in 2021.

In this context, numerical simulation stands out as a key tool for better understanding, predicting, and managing these phenomena. It allows to account for coupled multiphysical processes underlying induced seismicity, evaluating the potential impacts of human activities on the subsurface, and designing strategies to minimize associated risks. At sufficiently large spatial scales, the models are based on a represention of the faults as interfaces equipped with mechanical properties (normal stiffness, friction laws, etc.) and hydraulic properties (aperture and hydraulic conductivity). The physical model couples Darcian fluid flow in the porous matrix and the fault network, the poro-elastic deformation of the rock in the matrix domain, as well as the highly nonlinear frictional slip laws along the fault network. An essential feature is the dynamic nature of the friction law, commonly described by a Rate and State law [4, 7] and for which the friction coefficient depends on the slip velocity and a fault state variable. The decrease of the normal traction with the fault pressure is the source of the potential fault reactivation which can further accelerate slip and induce seismicity when the friction coefficient and consequently the resistance to slip decreases with the slip velocity.

This work presents a polytopal discretisation to simulate these coupled processes, taking into account 3D fault networks and dynamic rate and state friction laws. The spatial discretisation is polytopal to cope with the complexity of geological meshes. It is based on the mixed Virtual Element Method

with bubble stabilisation introduced in [2] and here extended to quasi-dynamic models. The mixed-dimensional Darcy flow model is discretised with an Hybrid Finite Volume scheme [1]. It is combined with an adaptive time integration in order to capture the very large time scale contrasts (up to 6 orders of magnitude) between the different phases of induced seismicity, ranging from pressure buildup to slip onset, from aseismic slip to seismic slip, and finally to slip arrest.

2 Quasi-dynamic poromechanical model

We let $\Omega \subset \mathbb{R}^d$, $d \in \{2,3\}$, denote a bounded polytopal domain, partitioned into a fault domain Γ and a matrix domain $\Omega\backslash\overline{\Gamma}$. The network of fractures is defined by $\overline{\Gamma} = \bigcup_{i\in I}\overline{\Gamma}_i$, where each fracture $\Gamma_i \subset \Omega$, $i \in I$ is a planar polygonal simply connected open domain (see Figure 2). The two sides of a given fracture of Γ are denoted by $\pm$ in the matrix domain, with unit normal vectors $\underline{n}^{\pm}$ oriented outward from the sides $\pm$. We denote by $\gamma_{\mathfrak{a}}$ the trace operators on the side $\mathfrak{a} \in \{+,-\}$ of Γ for functions in $H^1(\Omega\backslash\overline{\Gamma})^d$ and by $\gamma_n^{\mathfrak{a}}$ the normal trace operator for functions in $H_{\mathrm{div}}(\Omega\backslash\overline{\Gamma})^d$. The jump operator on Γ for functions $\underline{u}$ in $(H^1(\Omega\backslash\overline{\Gamma}))^d$ is defined by

$$[\![\underline{u}]\!] = \gamma_+\underline{u} - \gamma_-\underline{u},$$

and we denote by $[\![\underline{u}]\!]_n = [\![\underline{u}]\!]\cdot\underline{n}^+$ and $[\![\underline{u}]\!]_{\boldsymbol{\tau}} = [\![\underline{u}]\!] - [\![\underline{u}]\!]_n\underline{n}^+$ its normal and tangential components. The

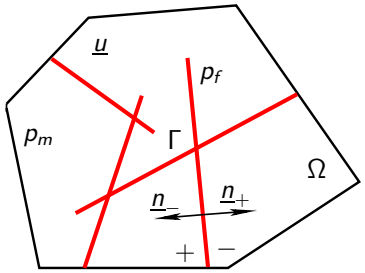

FIGURE 1 – Model representing the fault network as interfaces with the main variables of the model, namely the displacement field $\underline{u}$, the pressures in the matrix p_m, and in the fault network p_f.

symmetric gradient operator $\underline{\underline{\varepsilon}}$ is defined such that $\underline{\underline{\varepsilon}}(\underline{v}) = \frac{1}{2}(\underline{\underline{\nabla}}\,\underline{v} + (\underline{\underline{\nabla}}\,\underline{v})^t)$ for a given vector field $\underline{v} \in H^1(\Omega\backslash\overline{\Gamma})^d$. Let $\underline{S}$ denote the slip and $\underline{\dot{S}} = \partial_t\underline{S}$ the slip velocity along the fracture network Γ, the quasi-dynamic model [7, 6, 3] couples the mechanical equilibrium at given jumps

$$\begin{cases} -\underline{\mathrm{div}}\,\underline{\underline{\sigma}}^\top(\underline{u},p_m) &= \underline{f} & \text{on } (0,T)\times\Omega\backslash\overline{\Gamma},\\ \underline{\underline{\sigma}}^\top(\underline{u}) &= \mathbb{A}\underline{\underline{\varepsilon}}(\underline{u}) - \alpha p_m\,\underline{\underline{I}} & \text{on } (0,T)\times\Omega\backslash\overline{\Gamma},\\ \underline{T}^+ + \underline{T}^- &= 0 & \text{on } (0,T)\times\Gamma,\\ [\![\underline{u}]\!]_n &= G & \text{on } (0,T)\times\Gamma,\\ [\![\underline{u}]\!]_{\boldsymbol{\tau}} &= \underline{S} & \text{on } (0,T)\times\Gamma, \end{cases} \tag{1}$$

with boundary conditions on the fractures that combine Rate and State Friction (RSF) under the aging state law and the radiation damping approximation to elastodynamic stress changes caused by seismic wave radiation :

$$\begin{cases} \underline{T}_{\boldsymbol{\tau}} = T_n\,F_{RSF}(|\underline{\dot{S}}|,\theta)\,\dfrac{\underline{\dot{S}}}{|\underline{\dot{S}}|} - \eta\underline{\dot{S}} & \text{on } (0,T)\times\Gamma,\\ \partial_t\theta = 1 - \dfrac{|\underline{\dot{S}}|\theta}{d_c} & \text{on } (0,T)\times\Gamma, \end{cases} \tag{2}$$

using the regularized RSF model

$$F_{RSF}(w,\theta) = a\,\mathrm{arcsinh}\left[\frac{w}{2v_0}\exp\left(\frac{1}{a}(f_0 + b\ln(\frac{v_0\,\theta}{d_c})\right)\right]. \tag{3}$$

In the equations above, θ denotes the state variable accounting for the maturity of the fault asperities, η is the radiation damping coefficient, G is the gap function, a, b, d_c, f_0, v_0 are the given RSF parameters along the fault, α is the Biot coefficient, and $\mathbb{A}$ is the fourth order elasticity tensor. In (1) and (2) the contact tractions are defined by

$$\begin{cases} \underline{T}^{\mathfrak{a}} = \gamma_n^{\mathfrak{a}} \underline{\sigma}^{\top}(\underline{u}, p_m) + p_f \underline{n}^{\mathfrak{a}} & \text{on } (0,T)\times\Gamma, \mathfrak{a}\in\{+,-\}, \\ T_n = \underline{T}^{+}\cdot\underline{n}^{+}, & \text{on } (0,T)\times\Gamma, \\ \underline{T}_{\boldsymbol{\tau}} = \underline{T}^{+} - (\underline{T}^{+}\cdot\underline{n}^{+})\underline{n}^{+} & \text{on } (0,T)\times\Gamma. \end{cases}$$

The quasi-dynamic model (1)-(2) is coupled to the following mixed-dimensional Darcy flow

$$\begin{cases} \partial_t \phi_m + \operatorname{div}\underline{V}_m = h_m & \text{on } (0,T)\times\Omega\backslash\overline{\Gamma}, \\ \underline{V}_m = -\frac{\mathbb{K}_m}{\mu_f}(\underline{\nabla} p_m - \rho \underline{g}) & \text{on } (0,T)\times\Omega\backslash\overline{\Gamma}, \\ \partial_t \mathrm{d}_f + \operatorname{div}_{\boldsymbol{\tau}}\underline{V}_f - [\![\underline{V}_m]\!]_n = h_f & \text{on } (0,T)\times\Gamma, \\ \underline{V}_f = -\frac{C_f}{\mu_f}(\underline{\nabla}_{\boldsymbol{\tau}} p_f - \rho \underline{g}_{\boldsymbol{\tau}}), & \text{on } (0,T)\times\Gamma, \\ \gamma_n^{\pm}\underline{V}_m^{\pm} = \Lambda_f(\gamma^{\pm} p_m - p_f + \frac{\mathrm{d}_f}{2}\rho\underline{g}\cdot\underline{n}^{\pm}) & \text{on } (0,T)\times\Gamma. \end{cases} \tag{4}$$

In the above formulation (4), μ_f represents the dynamic viscosity of the fluid, ϕ_m is the porosity of the matrix, $\mathbb{K}_m$ denotes the permeability tensor of the matrix, ρ the fluid constant specific density, and $\underline{g}$ the acceleration of gravity vector. The terms h_m and h_f on the right-hand side represent fluid injection or production sources. The fracture aperture d_f determines the fracture conductivity C_f following typically the Poiseuille law $C_f = \mathrm{d}_f^3/12$. Similarly, the fracture normal transmissivity Λ_f is defined as $2K_{f,\underline{n}}/\mathrm{d}_f$, with $K_{f,\underline{n}}$ representing the normal permeability of the fracture.

The model is completed by typically assuming that the pressure p_f is continuous at fracture intersections and by boundary conditions on p_m along $\partial\Omega$ and on p_f along $\partial\Gamma\cap\partial\Omega$. Homogeneous Neumann boundary conditions are classically applied to p_f at the fracture tips on $\partial\Gamma\backslash\partial\Omega$.

The poromechanical model (1)-(2)-(4) is closed by the following coupling laws

$$\begin{cases} \partial_t \phi_m = \alpha \operatorname{div}(\partial_t \underline{u}) + \frac{1}{M}\partial_t p_m & \text{on } (0,T)\times\Omega\backslash\overline{\Gamma}, \\ \partial_t \mathrm{d}_f = -\partial_t [\![\underline{u}]\!]_n & \text{on } (0,T)\times\Gamma. \end{cases} \tag{5}$$

The first equation accounts for the linear isotropic poroelastic constitutive law for the porosity ϕ_m, with M denoting the Biot modulus. The second equation specifies the fracture aperture d_f. Note that since the model assumes a contact state, we have $[\![\underline{u}]\!]_n = G$.

The gap function models the mechanical behavior of the fault asperities. It typically accounts for shear dilation using the gap function $G(\underline{u}) = -\tan(\psi)|[\![\underline{u}-\underline{u}^0]\!]_{\boldsymbol{\tau}}|$, where ψ is the shear dilation angle. It can additionally account for normal compliance with $G(\underline{u}, T_n) = -\frac{T_n}{K_n} - \tan(\psi)|[\![\underline{u}-\underline{u}^0]\!]_{\boldsymbol{\tau}}|$, where K_n is the fault normal stiffness, and $\underline{u}^0$ is the initial displacement field.

3 Space and time discretisations

3.1 VEM-bubble space discretisation of the quasi-dynamic model

The space discretisation of the quasi-dynamic model is based on the VEM-bubble nodal polytopal method introduced in [2] for quasi static contact-mechanical models with Coulomb friction. This discretisation is based on a mixed formulation using facewise constant Lagrange multipliers along the fault and the first order nodal polytopal Virtual Element Method (VEM) for the displacement field stabilised by discrete vectorial bubble unknowns on one side of each fracture face. This method has the advantage of leading to a diagonal coupling operator for contact, which facilitates its coupling with dynamic friction models on general fracture networks.

3.1.1 Polytopal mesh and discrete spaces

We consider a polyhedral mesh of the domain Ω, conforming to the fracture network Γ. For each cell K, we denote by h_K its diameter and by $|K|$ its measure; we also denote by $|\sigma|$ the $(d-1)$-dimensional

measure of a face σ. The set of cells K, the set of faces σ, the set of edges e and the set of nodes s are denoted respectively by $\mathcal{M}$, $\mathcal{F}$, $\mathcal{E}$ and $\mathcal{V}$. Let us denote by $\mathcal{F}_K$ and $\mathcal{V}_K$ the set of faces and nodes of a cell K, by $\mathcal{E}_\sigma$ the set of edges of a face σ, and by $\mathcal{M}_\sigma$ the set of cells that contain the face σ We assume the existence of a subset of faces $\mathcal{F}_\Gamma \subset \mathcal{F}$ such that $\overline{\Gamma} = \bigcup_{\sigma\in\mathcal{F}_\Gamma} \overline{\sigma}$. The mesh is assumed conforming in the sense that the set $\mathcal{M}_\sigma$ of neighboring cells of $\sigma \in \mathcal{F}$ is either $\mathcal{M}_\sigma = \{K, L\}$ for an interior face $\sigma \in \mathcal{F}^{\rm int}$ (in which case we write $\sigma = K|L$), or $\mathcal{M}_\sigma = \{K\}$ for a boundary face $\sigma \in \mathcal{F}^{\rm ext}$. It is assumed that $\mathcal{F}_\Gamma \subset \mathcal{F}^{\rm int}$ and, if $\sigma = K|L$, that K and L are ordered such that $\underline{n}_{K\sigma} = \underline{n}^+$ and $\underline{n}_{L\sigma} = \underline{n}^-$, where $\underline{n}_{K\sigma}$ (resp. $\underline{n}_{L\sigma}$) is the unit normal vector to σ oriented outward of K (resp. L).

We denote by $\mathcal{V}^{\rm ext}$ and $\mathcal{E}^{\rm ext}$ the boundary nodes and edges. For each $\sigma \in \mathcal{F}$, $\underline{n}_{\sigma e}$ is the unit normal vector to $e \in \mathcal{E}_\sigma$ in the plane spanned by σ oriented outward to σ.

The degrees of freedom (DOFs) for the displacement are nodal (attached to the vertices of the mesh), but could be discontinuous across the fracture network. To be more specific, let us first define a partition $\overline{\mathcal{M}_s}$ of the set of cells $\mathcal{M}_s$ around a given node $s \in \mathcal{V}$. For a given cell $K \in \mathcal{M}_s$ we denote by $\mathcal{K}s \in \overline{\mathcal{M}_s}$ the subset of $\mathcal{M}_s$ such that $\bigcup_{L\in\mathcal{K}s} \overline{L}$ is the closure of the connected component of $(\bigcup_{L\in\mathcal{M}_s} \overline{L}) \setminus \Gamma$ containing the cell K. In other words, $\mathcal{K}s$ is the set of cells in $\mathcal{M}_s$ that are on the same side of Γ as K. A nodal displacement unknown $\underline{v}_{\mathcal{K}s}$ is defined for each $\mathcal{K}s \in \overline{\mathcal{M}_s}$. Let us note that there is a unique nodal displacement unknown $\underline{v}_{\mathcal{K}s}$ at a node s not belonging to Γ, since $\overline{\mathcal{M}_s} = \mathcal{M}_s$ in that case. On the other hand, for a fracture node s, the nodal displacement unknown $\underline{v}_{\mathcal{K}s}$ is the one on the side K of the set of fractures connected to s. Additionally, on the positive side of the fracture, we attach to each face a vector DOF corresponding to a "correction" of the face values generated by the nodal DOFs; this correction plays the role, at the discrete level represented by the space of DOFs, of a bubble function and is introduced to ensure a suitable inf–sup condition between the space of Lagrange multipliers and the jump of the displacements.

For each $K \in \mathcal{M}$, we denote by

$$\mathcal{F}_{\Gamma,K}^+ = \left\{\sigma \in \mathcal{F}_\Gamma \cap \mathcal{F}_K : \underline{n}_{K\sigma} \cdot \underline{n}^+ > 0\right\}$$

the set of faces of K that lie on the positive side of Γ (that set is empty if K does not touch Γ or only touches it from its negative side). According to the discussion above, the discrete space of displacement is

$$\mathbf{U}_h = \left\{\underline{v}_h = ((\underline{v}_{\mathcal{K}s})_{\mathcal{K}s\in\overline{\mathcal{M}_s}, s\in\mathcal{V}}, (\underline{v}_{K\sigma})_{K\in\mathcal{M},\sigma\in\mathcal{F}_{\Gamma,K}^+}) : \underline{v}_{\mathcal{K}s} \in \mathbb{R}^d,\ \underline{v}_{K\sigma} \in \mathbb{R}^d\right\},$$

with

$$\mathbf{U}_{h,0} = \left\{\underline{v}_h \in \mathbf{U}_h : \underline{v}_{\mathcal{K}s} = \underline{0} \text{ if } s \in \mathcal{V}^{\rm ext}\right\}. \tag{6}$$

The Lagrange multiplier plays the role of approximations of $\underline{T}$ on Γ. Its space is made of piecewise constant vectors :

$$\mathbf{M}_h = \left\{\underline{\lambda}_h \in \boldsymbol{L}^2(\Gamma) : \underline{\lambda}_\sigma := (\underline{\lambda}_h)_{|\sigma} \text{ is constant for all } \sigma \in \mathcal{F}_\Gamma\right\}.$$

For $\underline{\lambda}_h \in \mathbf{M}_h$, we define its normal and tangential components by

$$\lambda_{h,n} = \underline{\lambda}_h \cdot \underline{n}^+, \quad \underline{\lambda}_{h,\boldsymbol{\tau}} = \underline{\lambda}_h - \lambda_{h,n}\underline{n}^+.$$

Let us refer to Figure 2 for an illustration of the displacement and Lagrange multiplier discrete unknowns.

3.1.2 Reconstruction operators in $\mathbf{U}_{h,0}$

We first define, for each $K \in \mathcal{M}$ and $\sigma \in \mathcal{F}_K$, a tangential face gradient $\underline{\underline{\nabla}}^{K\sigma} : \mathbf{U}_{h,0} \to \mathbb{P}^0(\sigma)^{d\times d}$ and tangential displacement reconstruction $\underline{\Pi}^{K\sigma} : \mathbf{U}_{h,0} \to \mathbb{P}^1(\sigma)$. First, we choose nonnegative weights $(\omega_s^\sigma)_{s\in\mathcal{V}_\sigma}$ to express the center of mass $\overline{\underline{x}}_\sigma$ of σ in terms of its vertices $\overline{\underline{x}}_\sigma = \sum_{s\in\mathcal{V}_\sigma} \omega_s^\sigma \underline{x}_s$, $\quad \sum_{s\in\mathcal{V}_\sigma} \omega_s^\sigma = 1$. Then, for $\underline{v}_h \in \mathbf{U}_{h,0}$, we set

$$\begin{aligned}
\underline{\underline{\nabla}}^{K\sigma}\underline{v}_h &= \frac{1}{|\sigma|}\sum_{e=s_1s_2\in\mathcal{E}_\sigma} |e| \frac{\underline{v}_{\mathcal{K}s_1} + \underline{v}_{\mathcal{K}s_2}}{2} \otimes \underline{n}_{\sigma e},\\
\underline{\Pi}^{K\sigma}\underline{v}_h(\underline{x}) &= \underline{\underline{\nabla}}^{K\sigma}\underline{v}_h(\underline{x} - \overline{\underline{x}}_\sigma) + \overline{\underline{v}}_{K\sigma} \quad \forall \underline{x} \in \sigma, \qquad \text{where } \overline{\underline{v}}_{K\sigma} = \sum_{s\in\mathcal{V}_\sigma} \omega_s^\sigma \underline{v}_{\mathcal{K}s}.
\end{aligned} \tag{7}$$

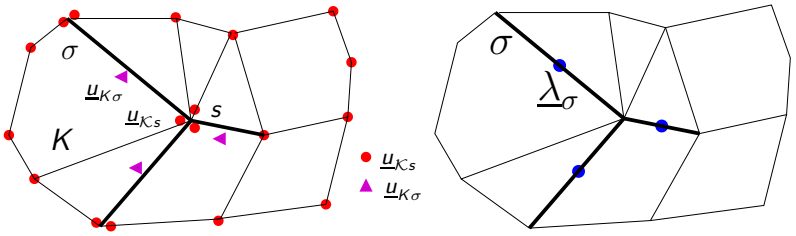

FIGURE 2 – Example of discrete nodal $\underline{u}_{\mathcal{K}s}$ and bubble $\underline{u}_{K\sigma}$ displacement unknowns, and of Lagrange Multiplier unknown $\underline{\lambda}_\sigma$.

Above, we have noted $e = s_1 s_2$ to indicate that the edge e has vertices s_1, s_2.

If $\sigma \in \mathcal{F}_\Gamma$ is a fracture face, and K (resp. L) is the cell on the positive (resp. negative) side of σ, we define the displacement jump operator on σ as $[\![\cdot]\!]_\sigma : \mathbf{U}_{h,0} \to \mathbb{P}^0(\sigma)^d$ such that, for all $\underline{v}_h \in \mathbf{U}_{h,0}$,

$$[\![\underline{v}_h]\!]_\sigma = \frac{1}{|\sigma|}\int_\sigma (\underline{\Pi}^{K\sigma}\underline{v}_h - \underline{\Pi}^{L\sigma}\underline{v}_h) + \underline{v}_{K\sigma} = \underline{\overline{v}}_{K\sigma} - \underline{\overline{v}}_{L\sigma} + \underline{v}_{K\sigma}. \tag{8}$$

The normal component of that jump is denoted by $[\![\cdot]\!]_{\sigma,n} = [\![\cdot]\!]_\sigma \cdot \underline{n}_{K\sigma}$.

For each cell $K \in \mathcal{M}$, we select nonnegative weights $(\omega_s^K)_{s\in\mathcal{V}_K}$ of a linear decomposition of the center of mass $\underline{\overline{x}}_K$ of K in terms of its vertices $\underline{\overline{x}}_K = \sum_{s\in\mathcal{V}_K} \omega_s^K \underline{x}_s$, $\sum_{s\in\mathcal{V}_K} \omega_s^K = 1$, and we design a gradient reconstruction $\underline{\underline{\nabla}}^K : \mathbf{U}_{h,0} \to \mathbb{P}^0(K)^{d\times d}$ and a displacement reconstruction $\underline{\Pi}^K : \mathbf{U}_{h,0} \to \mathbb{P}^1(K)^d$ by setting, for $\underline{v}_h \in \mathbf{U}_{h,0}$,

$$\underline{\underline{\nabla}}^K \underline{v}_h = \frac{1}{|K|}\sum_{\sigma\in\mathcal{F}_K} |\sigma| \underline{\overline{v}}_{K\sigma} \otimes \underline{n}_{K\sigma} + \sum_{\sigma\in\mathcal{F}^+_{\Gamma,K}} \frac{|\sigma|}{|K|} \underline{v}_{K\sigma} \otimes \underline{n}_{K\sigma}, \tag{9}$$

$$\underline{\Pi}^K \underline{v}_h(\underline{x}) = \underline{\underline{\nabla}}^K \underline{v}_h(\underline{x} - \underline{\overline{x}}_K) + \underline{\overline{v}}_K \quad \forall \underline{x} \in K, \qquad \text{where } \underline{\overline{v}}_K = \sum_{s\in\mathcal{V}_K} \omega_s^K \underline{v}_{\mathcal{K}s}. \tag{10}$$

These local jump, gradient and displacement reconstructions are patched together to create their global piecewise polynomial counterparts $[\![\cdot]\!]_h : \mathbf{U}_{h,0} \to \mathbb{P}^0(\mathcal{F}_\Gamma)^d$, $\underline{\underline{\nabla}}^h : \mathbf{U}_{h,0} \to \mathbb{P}^0(\mathcal{M})^{d\times d}$ and $\underline{\Pi}^h : \mathbf{U}_{h,0} \to \mathbb{P}^1(\mathcal{M})^d$: for all $\underline{v}_h \in \mathbf{U}_{h,0}$,

$$([\![\underline{v}_h]\!]_h)_{|\sigma} = [\![\underline{v}_h]\!]_\sigma \qquad \forall \sigma \in \mathcal{F}_\Gamma, \quad (\underline{\underline{\nabla}}^h \underline{v}_h)_{|K} = \underline{\underline{\nabla}}^K \underline{v}_h \qquad \forall K \in \mathcal{M}, \quad (\underline{\Pi}^h \underline{v}_h)_{|K} = \underline{\Pi}^K \underline{v}_h \qquad \forall K \in \mathcal{M}.$$

We also define the cellwise constant reconstruction operator $\underline{\widetilde{\Pi}}^h \underline{v}_h : \mathbf{U}_{h,0} \to \mathbb{P}^0(\mathcal{M})^d$ such that $(\underline{\widetilde{\Pi}}^h \underline{v}_h)_{|K} = \underline{\overline{v}}_K$. Finally, the discrete symmetric gradient $\underline{\underline{\varepsilon}}_h(.)$, divergence $\mathrm{div}_h(.)$ and stress tensor $\varpi_h(.,.)$ are deduced from the previous operators :

$$\underline{\underline{\varepsilon}}_h = \frac{1}{2}(\underline{\underline{\nabla}}^h + (\underline{\underline{\nabla}}^h)^t), \quad \mathrm{div}_h = \mathrm{Tr}\left(\underline{\underline{\varepsilon}}_h\right) \quad \text{and} \quad \underline{\underline{\sigma}}_h(\underline{u}_h) = \mathbb{A}\underline{\underline{\varepsilon}}_h(\underline{u}_h),$$

where Tr denotes the trace operator.

3.1.3 Mixed-variational formulation

We now introduce the numerical scheme for the mixed-variational formulation of the mechanical problem (1) : given $\underline{S}_h \in \mathbf{M}_h$, and the respectively cellwise contant and fracture facewise constant matrix and fault discrete pressures $(\Pi_h^m p_h^m, \Pi_h^f p_h^f)$, find $(\underline{u}_h, \underline{\lambda}_h) \in \mathbf{U}_{h,0} \times \mathbf{M}_h$ such that, for all $(\underline{v}_h, \underline{\mu}_h) \in \mathbf{U}_{h,0} \times \mathbf{M}_h$,

$$\begin{aligned} &\int_\Omega \underline{\underline{\sigma}}_h(\underline{u}_h) : \underline{\underline{\varepsilon}}_h(\underline{v}_h) + S_{\mathbb{A},h}(\underline{u}_h, \underline{v}_h) - \int_\Omega \alpha\, \Pi_h^m p_h^m\ \mathrm{div}_h \underline{v}_h \\ &+ \int_\Gamma \Pi_h^f p_h^f\ [\![\underline{v}_h]\!]_{h,n} + \int_\Gamma \underline{\lambda}_h \cdot [\![\underline{v}_h]\!]_h = \int_\Omega \underline{f} \cdot \underline{\widetilde{\Pi}}^h \underline{v}_h, \\ &\int_\Gamma \mu_{h,n}\ ([\![\underline{u}_h]\!]_{h,n} - G) + \int_\Gamma \underline{\mu}_{h,\boldsymbol{\tau}} \cdot ([\![\underline{u}_h]\!]_{h,\boldsymbol{\tau}} - \underline{S}_h) = 0. \end{aligned} \tag{11}$$

Here, $S_{\mathbb{A},h}$ is the scaled stabilisation bilinear form defined by

$$S_{\mathbb{A},h}(\underline{u}_h, \underline{v}_h) = \sum_{K\in\mathcal{M}} |K| \mathrm{A}_K S_K(\underline{u}_h, \underline{v}_h)$$

where $\mathrm{A}_K = \frac{1}{|K|}\max_{i,j,k,l}\int_K \mathbb{A}_{i,j,k,l}d\underline{x}$, and with local stabilisation bilinear form $S_K : \mathbf{U}_{h,0}\times\mathbf{U}_{h,0}\to\mathbb{R}$ given by

$$S_K(\underline{u}_h, \underline{v}_h) = h_K^{-2}\sum_{s\in\mathcal{V}_K}\left(\underline{u}_{\mathcal{K}s} - \underline{\Pi}^K\underline{u}_h(\underline{x}_s)\right)\cdot\left(\underline{v}_{\mathcal{K}s} - \underline{\Pi}^K\underline{v}_h(\underline{x}_s)\right) + h_K^{-2}\sum_{\sigma\in\mathcal{F}_{\Gamma,K}^+}\underline{u}_{K\sigma}\cdot\underline{v}_{K\sigma}. \tag{12}$$

3.2 Mixed-dimensional Darcy flow space discretisation

We consider the Hybrid Finite Volume (HFV) discretisation of the mixed-dimensional Darcy flow model introduced in [1]. It is based on the vector space $X_h = X_h^m \times X_h^f$ of discrete pressures $p_h = (p_h^m, p_h^f)$ (see Figure 3) defined by

$$X_h^m = \left\{p_h^m = \left((p_K)_{K\in\mathcal{M}}, (p_\sigma)_{\sigma\in\mathcal{F}\setminus\mathcal{F}_\Gamma}, (p_{K\sigma})_{\sigma\in\mathcal{F}_\Gamma, K\in\mathcal{M}_\sigma}\right) : p_K\in\mathbb{R},\ p_\sigma\in\mathbb{R},\ p_{K\sigma}\in\mathbb{R}\right\}, \tag{13}$$

$$X_h^f = \left\{p_h^f = \left((p_\sigma)_{\sigma\in\mathcal{F}_\Gamma}, (p_e)_{e\in\mathcal{E}_\Gamma}\right) : p_\sigma\in\mathbb{R},\ p_e\in\mathbb{R}\right\}. \tag{14}$$

Assuming for simplicity homogeneous Dirichlet boundary conditions, we denote by $X_{h,0}^m$ (resp. $X_{h,0}^f$) the subspace of X_h^m (resp. X_h^f) with vanishing values at the boundary $\mathcal{F}^{\mathrm{ext}}$ (resp. $\mathcal{E}^{\mathrm{ext}}\cap\mathcal{E}_\Gamma$), and we set $X_{h,0} = X_{h,0}^m\times X_{h,0}^f$. The HFV scheme is obtained by replacing, in the primal variational formulation of

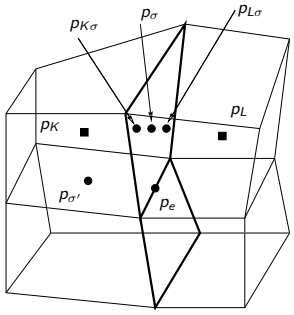

FIGURE 3 – Illustration of the Hybrid Finite Volume (HFV) matrix (p_K, $p_{\sigma'}$, $p_{K\sigma}$, p_L, $p_{L\sigma}$) and fracture (p_σ, p_e) discrete pressure unknowns.

(4), the continuous operators by discrete reconstruction operators $\underline{\nabla}_h^m$, Π_h^m, $\mathbb{T}_h^{m,\pm}$ in the matrix and $\underline{\nabla}_h^f$, Π_h^f along the fractures, defined as follows.

The matrix gradient reconstruction operator $\underline{\nabla}_h^m : X_h^m \longrightarrow L^2(\Omega)^d$ is such that, for a suitable symmetric positive definite tensor $\mathbb{T}_K = (\mathbb{T}_K^{\nu\nu'})_{(\nu,\nu')\in I_K\times I_K}$, for all $p_h^m\in X_h^m$,

$$\int_K \mathbb{K}_m\underline{\nabla}_h^m p_h^m\cdot\underline{\nabla}_h^m q_h^m = \sum_{\nu\in I_K}\sum_{\nu'\in I_K}\mathbb{T}_K^{\nu\nu'}(p_\nu - p_K)(q_{\nu'} - q_K) \qquad \forall q_h^m\in X_h^m,$$

with

$$I_K = \{\sigma\in\mathcal{F}_K\setminus\mathcal{F}_\Gamma\}\cup\{K\sigma,\ \sigma\in\mathcal{F}_K\cap\mathcal{F}_\Gamma\},$$

denoting the subset of matrix degrees of freedom (DOFs) located at the boundary of the cell K. The fracture tangential gradient operator $\underline{\nabla}_h^f : X_h^f \longrightarrow L^2(\Gamma)^{d-1}$ is such that, for a suitable symmetric positive definite tensor $\mathbb{T}_\sigma = (\mathbb{T}_\sigma^{ee'})_{(e,e')\in\mathcal{E}_\sigma\times\mathcal{E}_\sigma}$, for all $p_h^f\in X_h^f$,

$$\int_\sigma C_{f,h}\underline{\nabla}_h^f p_h^f\cdot\underline{\nabla}_h^f q_h^f = \sum_{e\in\mathcal{E}_\sigma}\sum_{e'\in\mathcal{E}_\sigma}\mathbb{T}_\sigma^{ee'}(p_{e'} - p_\sigma)(q_e - q_\sigma) \qquad \forall q_h^f\in X_h^f,$$

with the face-wise constant approximation of the fracture conductivity given by $C_{f,h} = \frac{(\mathrm{d}_{f,h})^3}{12}$, where $\mathrm{d}_{f,h}$ is the face-wise constant approximation of the fracture aperture specified in (16). The detailed definitions of $\mathbb{T}_K$ and $\mathbb{T}_\sigma$ can be found in [1].

The piecewise constant matrix and fracture function reconstruction operators $\Pi_h^m : X_h^m \to L^2(\Omega)$ and $\Pi_h^f : X_h^f \to L^2(\Gamma)$ are defined by

$$\Pi_h^m q_h^m(\underline{x}) = q_K,\ \forall \underline{x} \in K,\ K \in \mathcal{M}, \qquad \Pi_h^f q_h^f(\underline{x}) = q_\sigma,\ \forall \underline{x} \in \sigma,\ \sigma \in \mathcal{F}_\Gamma,$$

and the face-wise constant sided trace reconstruction operators $\mathbb{T}_h^{m,\pm} : X_h \to L^2(\Gamma)$ by

$$\mathbb{T}_h^{m,+} q_h^m(\underline{x}) = q_{K\sigma}, \quad \mathbb{T}_h^{m,-} q_h^m(\underline{x}) = q_{L\sigma}, \quad \forall \underline{x} \in \sigma = K|L, \sigma \in \mathcal{F}_\Gamma.$$

Let us also define the face-wise constant approximation of the fracture normal transmissivity $\Lambda_{f,h} = \frac{2K_{f,\underline{n}}}{\mathrm{d}_{f,h}}$. Finally, for the gravity terms, let us define $g = |\underline{g}|$ and

$$z_h^m = \Big((z_K)_{K\in\mathcal{M}}, (z_\sigma)_{\sigma\in\mathcal{F}\setminus\mathcal{F}_\Gamma}, (z_{K\sigma})_{\sigma\in\mathcal{F}_\Gamma, K\in\mathcal{M}_\sigma}\Big), \qquad z_h^f = \Big((z_\sigma)_{\sigma\in\mathcal{F}_\Gamma}, (z_e)_{e\in\mathcal{E}_\Gamma}\Big),$$

where z_ν denotes the vertical coordinate of the center of mass of ν, taking into account the fracture width for $\nu = K\sigma$. Then, the HFV scheme can be expressed as the following discrete variational formulation : find $p_h : [0,T] \to X_h^0$ such that, for all $q_h : [0,T] \to X_h^0$, it holds

$$\begin{aligned}
&\int_\Omega \Big((\partial_t \phi_h)\Pi_h^m q_h^m + \frac{\mathbb{K}_m}{\mu_f}\underline{\nabla}_h^m(p_h^m + \rho g z_h^m)\cdot\underline{\nabla}_h^m q_h^m\Big) + \int_\Gamma \Big((\partial_t \mathrm{d}_{f,h})\Pi_h^f q_h^f + \frac{C_{f,h}}{\mu_f}\underline{\nabla}_h^f(p_h^f + \rho g z_h^f)\cdot\underline{\nabla}_h^f q_h^f\Big) \\
&+ \sum_{\mathfrak{a}\in\{+,-\}} \int_\Gamma \Lambda_{f,h}\Big(\mathbb{T}_h^{m,\mathfrak{a}}(p_h^m + \rho g z_h^m) - \Pi_h^f(p_h^f + \rho g z_h^f)\Big)\Big(\mathbb{T}_h^{m,\mathfrak{a}} q_h^m - \Pi_h^f q_h^f\Big) = \int_\Omega h_m \Pi_h^m q_h^m + \int_\Gamma h_f \Pi_h^f q_h^f,
\end{aligned} \tag{15}$$

where the approximations of the porosity ϕ_h and fracture aperture $\mathrm{d}_{f,h}$ are defined by the following coupling laws

$$\begin{aligned}
&\partial_t \phi_h = \alpha\ \mathrm{div}_h(\partial_t \underline{u}_h) + \tfrac{1}{M}\Pi_h^m \partial_t p_h^m, \\
&\partial_t \mathrm{d}_{f,h} = -\partial_t [\![\underline{u}_h]\!]_{h,\underline{n}},
\end{aligned} \tag{16}$$

defining the discrete porosity ϕ_h and fracture aperture $\mathrm{d}_{f,h}$, given a cellwise constant approximation ϕ_h^0 of the initial porosity ϕ^0 and a facewise constant approximation $\mathrm{d}_{f,h}^0$ of the initial aperture.

3.3 Time discretisation

Following [4, 7, 6, 3], the time integration of the quasi-dynamical model is based on the explicit adaptive Runge-Kutta Fehlberg RK45 time integration scheme. It is combined with an Euler implicit time integration for the Darcy flow. The coupling strategy between the quasi-dynamical and the Darcy flow models is still an ongoing work and will be based either on sequential or iterative coupling algorithms possibly using multirate time stepping. The solution algorithm involves the computation of the traction $\underline{\lambda}_h$ at given slip $\underline{S}_h$ at each substep of the RK45 scheme. This is achieved by solving the elasticity linear system reduced to the nodal unknowns with a fixed sparse Symmetric Positive Definite (SPD) matrix. In 2D this matrix can be factorised once and for all and the solution is obtained efficiently by a forward and backward substitution. In 3D an efficient preconditioner should be computed in preprocessing and the system solved by an iterative algorithm.

3.4 Numerical Validation of the scheme

The numerical model is validated using an induced seismicity community benchmark [5] which considers a 2-D antiplane problem for a planar fault embedded in a homogeneous unbounded space with rate and state friction and aging state laws. The fault slip is induced by the injection of fluid during 100 days in the middle of the fault. Fluid diffusion occurs only in the fault (impervious matrix) at fixed hydraulic aperture d_f and fault conductivity C_f leading to a one way coupled model. Figure 4 compares the maximum slip rate as a function of time obtained with our scheme (VB) to the reference solution from the benchmark. It exhibits a very good match on the finest mesh of size 100 m along the fault and roughly a first order convergence on a family of refined meshes as expected.

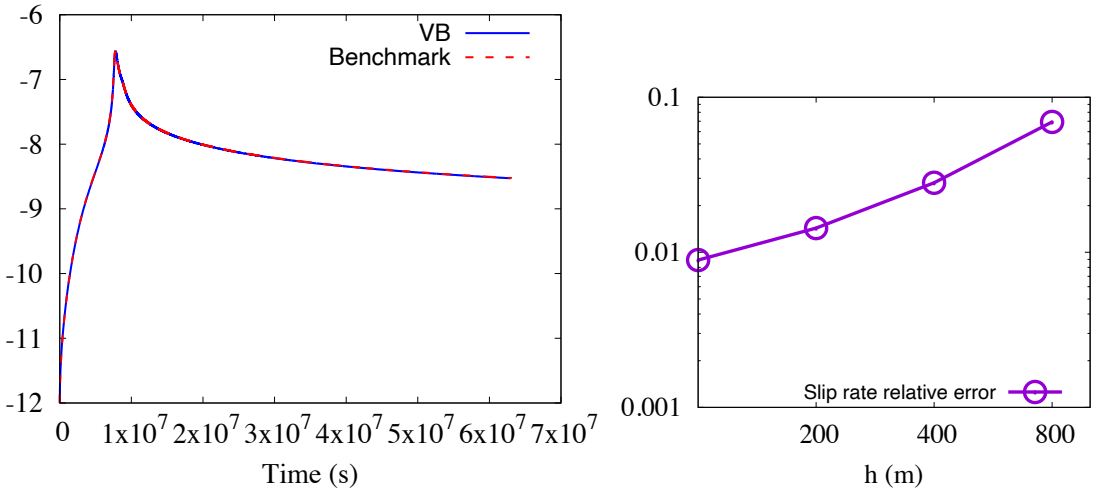

FIGURE 4 – (left) Comparison of the maximum slip rate in log10 scale as a function of time obtained with our scheme (VB) and with the reference benchmark. (right) Convergence of the relative error for the maximum slip rate evaluated w.r.t. the reference benchmark solution on a family of meshes of size h along the fault.

4 Conclusions and perspectives

This work presents the extension of a first order Virtual Element polytopal discretisation with bubble stabilisation to a quasi-dynamic poromechanical model with slip governed by a rate and state friction along the faults. It has been validated on an induced seismicity community benchmark. Ongoing works involve more advanced test cases with an heterogeneous matrix and fault networks, the development of coupling algorithms for fully coupled simulations with mechanical dependent fault aperture and conductivity, as well as 3D simulations requiring efficient precondioners for the elasticity SPD matrix. The code used for the simulations can be made available on demand.

Références

[1] K. Brenner, J. Hennicker, R. Masson, P. Samier, *Gradient Discretization of Hybrid Dimensional Darcy Flows in Fractured Porous Media with discontinuous pressure at matrix fracture interfaces*, IMA Journal of Numerical Analysis, 1551–1585, 2017.

[2] J. Droniou, G. Enchéry, I. Faille, A. Haidar, R. Masson, *A bubble VEM–fully discrete polytopal scheme for mixed-dimensional poromechanics with frictional contact at matrix-fracture interfaces*, Computer Methods in Applied Mechanics and Engineering, 2024.

[3] G. Gerardi, P. Dublanchet, L. Jeannin, A. Kazantsev, L. Duboeuf, I. Ramadhan, H. Azis, N. Ganefianto, I.A. Nugroho, *Geomechanical modelling of injection-induced seismicity : the case study of the Muara Laboh geothermal plant*, Geophysical Journal International,818-837, 2024.

[4] Y. Kaneko, J.-P. Ampuero, N. Lapusta, *Spectral-element simulations of long-term fault slip : Effect of low-rigidity layers on earthquake-cycle dynamics*, Journal of Geophysical Research : Solid Earth, 2011.

[5] V.R. Lambert, B.A. Erickson, J. Jiang, E. M. Dunham, T. Kim, J.-P. Ampuero et al, *Community-driven code comparisons for simulations of fluid-induced aseismic slip* Journal of Geophysical Research :Solid Earth, 130, 2025.

[6] P. Romanet, M.M. Scuderi, J.-P. Ampuero, S. Chaillat, F. Cappa. *Coupled Boundary Element and Finite Volume Methods for Modeling Fluid-Induced Seismicity in Fault Networks within Low-Permeability Rocks*, preprint hal-04343287, 2024.

[7] C. Uphoff, D.A May, A.-A. Gabriel, *A discontinuous Galerkin method for sequences of earthquakes and aseismic slip on multiple faults using unstructured curvilinear grids*, Geophysical Journal International, 586-626, 2022.